Evolution of Hierarchically Layered Cu-rich Silicide Nanoarchitectures

Ibrahim Saana Amiinu, Nilotpal Kapuria, Temilade Esther Adegoke, Angelika Holzinger, Hugh Geaney, Micheál D. Scanlon, Kevin M Ryan*

Bernal Institute, University of Limerick, Limerick, V94 T9PX, Ireland

Department of Chemical Sciences, University of Limerick, Limerick, V94 T9PX, Ireland

ABSTRACT: A solution based synthesis of well-ordered Cu-rich silicide nanoarchitectures, consisting of a pair of layered cups and stems (ρ-$Cu_{15}Si_4$) is demonstrated. The as-grown ρ-$Cu_{15}Si_4$ typically exhibits distinct interconnected 1D stems, consisting of a stack of nanorods (~300 nm in length), terminated with concave hexagonal 3D cups that evolve through a self-regulated layer-by-layer growth mechanism. Discrete-time *ex situ* experimental observations reveal that the ρ-$Cu_{15}Si_4$ evolution is driven by interatomic diffusion, initially triggering the formation of binary-phase silicide islands (spheres) followed by the formation of hexagonal discs, stem growth, and lateral elongation in exactly opposite directions. It is further shown that electrochemically pregrown Cu-crystals can facilitate the direct growth of ρ-$Cu_{15}Si_4$ in high yield with enhanced substrate coverage.

INTRODUCTION

Transition metal silicides (TMS) have a wide range of applications in applied science, arising from their inherent compatibility with Si and electronic properties that are compositionally tunable.[1-8] Common synthesis routes to TMS typically include the conversion of preformed Si structures coated with a desired metal precursor by annealing,[9,10,11] coprecipitation of precursor metal and Si atoms on

a discrete substrate,[12,13] or the direct reaction of Si monomers with a desired metal precursor substrate.[14,15] To date, a variety of TMS with tailored functional properties such as $MnSi_{1.7}$ and $CrSi_2$ (thermoelectrics),[16,17] β-$FeSi_2$ (optics),[18] Co_2MnSi (magnetics),[19] and low resistivity $NiSi_2$ or PtSi nanowires (NWs) for Schottky barriers and gas-sensing devices have been reported.[20,21]

Of particular interest are Cu-silicides, which are a promising class of materials with potential impact on several technological fronts, including uses as Cu-ion diffusion barriers, passivation layers, and lithium-ion battery current collectors.[14,15,22-26] By far, Cu_3Si and its polymorphs are the phases predominantly reported compared to the more attractive Cu-rich phase ($Cu_{15}Si_4$), and are typically synthesised *via* solid-state reactions, for example, by evaporation of Cu or CuO powders on Si wafers at high temperatures (650–900 ^oC) or by Au-catalyst assisted vapour transport mechanism at 960 ^oC.[27-29] These approaches have allowed the formation of asymmetric microfilms, which are squared, triangular, and nanorod shaped particles.[27-30] Single crystal Cu_3Si with defined growth positions have also been synthesised *via* a surface energy-driven mechanism at 650 ^oC.[1,28] The growth process relies on patterned defects on a Si substrate as nucleation centers and a Ge-catalyst to facilitate the surface diffusion process.[28] A more recent study of the growth mechanism of free-standing Cu_3Si NWs on a multilayered Cu/Ge/SiO_2/Si substrate identified the formation of isolated silicide islands as active sites for the NW growth.[27,29] Combined theoretical and experimental studies have also shown that a first-order phase transition occurs through the formation of an intermediate state, which significantly induces the creation of new-phase nuclei,[31] and that diffusional coalescence of islands on the crystal surface can promote faceting, indicating a layer-by-layer growth mechanism.[32] The Cu-rich phase ($Cu_{15}Si_4$) is highly desirable as it exhibits enhanced electrical and electronic properties, higher oxidation resistance and chemical stability, refined crystal structure, higher melting point (>800 ^oC), and the ability to reduce minority-carrier diffusion lengths, *e.g.* for efficient recombination in solar cells.[4,9,14,26] Thin films of $Cu_{15}Si_4$ have been achieved using solid Cu/Si elements *via* an arc-melting

technique.[26] In addition to the mixed formation of Cu_3Si intermediates, the procedure necessitates a further sample annealing treatment at 780 ^oC for up to 120 h.

It has been previously demonstrated that the delivery of Si monomer to a metal precursor substrate in high-boiling point organic solvents (HBOS) can effectively induce the direct growth of single-phase Cu-silicide NWs or axial heterostructured Ni-silicide NWs, thus, offering a new route to directly synthesise Cu-rich silicides at a lower temperature (460 ^oC) compared to an all-solid-state reaction procedure.[14,15] However, the process still depends on either a Au-catalyst to drive the silicidation process (heterostructures),[15,30] or the formation of underlying Cu-silicide seeds (as a self-generated catalyst) to activate the growth of the NWs.[14] The latter process is more complicated, as the latent formation of underlying silicide seeds can preferentially induce the growth of pure-phase Si NWs, through a vapour-solid-solid mechanism, with limited or no silicide NW formation.[14] Moreover, the silicide NW growth is nonuniform with disoriented multipod clusters in a wide morphology distribution, making insights into the growth mechanism difficult.[14,15,27,30]

Herein, for the first time we demonstrate an in-plane growth mechanism of well-ordered Cu-rich silicide nanostems terminated by a concave morphology (hereafter referred to as cup and stem) *via* a simple solution approach. Typically, the as-grown silicide (ρ-$Cu_{15}Si_4$) exhibits a pair (ρ) of interconnected 1D stems with node-internode-like features (a stack of nanorods) and concave hexagonal 3D cups that evolve through a self-regulated layer-by-layer growth mechanism. The ρ-$Cu_{15}Si_4$ was synthesised via two distinct approaches, as detailed in the supporting information. In the first case, a previously prepared planar Cu foil was directly used as the growth substrate, while in the second case, a single layer of pyramidal Cu-crystals were electrochemically grown on a Cu foil before being used as the growth substrate. The as-prepared substrates were then each subjected to similar silicidation process to reveal the prevailing growth mechanism.[33,34]

RESULTS AND DISCUSSION

Material structure and composition

Panels **a** and **b** in **Figure 1** show SEM images of the hierarchically grown pair of cup-stem architecture with the stems extending up to ~3.20 μm in length and ~150 nm in diameter. Interestingly, the stems share the same growth crystal base and elongate in exactly opposite directions with comparable topological features in terms of length, shape, and orientation. **Figure 1c** reveals that the stems consist of a stack of nanorods (~300 nm in length) interconnected in a fashion akin to the node-internode features of a bamboo stalk (**Figure S1**). As clearly seen in **Figure 1d**, the stem growth (nanorod stacking) is terminated by the formation of well-defined concave structures (cups). **Figure 1e** further reveals that the proliferation of the cup is facilitated by a diffusion-induced formation/deposition of concentric rings of hexagonal layers, stacked into a stair-like morphology, yielding a cup-like feature with sizes proportional to the number of layers (**Figure S2**). Previous reports have shown that such layered and stepwise growth features may be due to a 2D nucleation process occurring on the spherical crystal surface as more Si flux reacts with diffused Cu atoms from the silicides grains, leading to displaced atomic arrangements promoted by the mechanism of screw dislocation.[32-34] The average cup size across the outermost vertices and estimated average depth are ~1.21 μm and ~450 nm, respectively. The Gaussian-fitted size distributions of the hierarchically grown cups and stems are shown in **Figure 1f** and **g**, respectively, with the detailed dimensions illustrated in **Figure 1h.** Chemical composition analysis by energy dispersive X-ray (EDX) spectrum (**Figure S3**) and elemental mapping (**Figure 2i**) confirm the presence and uniform distribution of both Si and Cu in the stem and cup sections, indicating a uniform silicide structure. A cross-sectional analysis by focused ion beam (FIB) milling was also performed to further examine the ρ-$Cu_{15}Si_4$ morphology. As shown in **Figure S4**, the FIB-SEM sectioning shows that the dent is only limited to the cup section with the stems being fully solid structures.

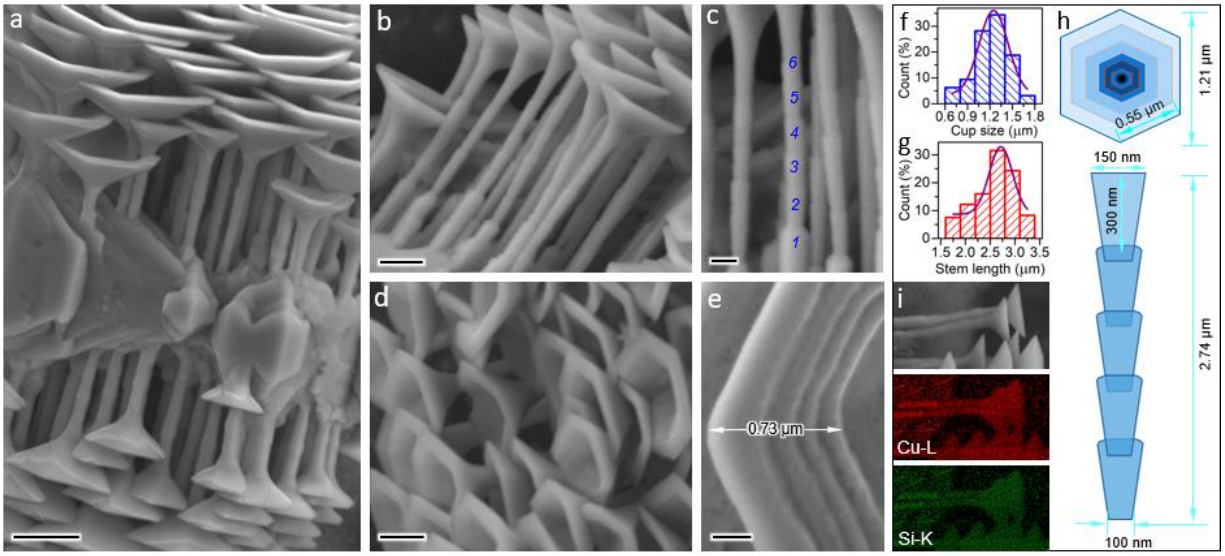

Figure 1 SEM images of the hierarchically grown ρ-$Cu_{15}Si_4$ architecture. (a) cups and stems feature extending in exactly opposite directions from the same growth crystal base (scale: 1µm), (b) selected area of stem-cup section (scale: 0.5 µm), (c) node-internode features of the stem (scale: 200 nm), numbers indicate the internodes, (d) cups (scale: 0.5 µm), and (e) stairs-like layered feature of the cup section (scale: 200 nm), and Gaussian-fitted size distribution histogram of (f) cups (average size: ~1.21± 0.5 µm) and (g) stems (average size: ~2.74 ± 0.6 µm), (h) Schematic illustration of the grown ρ-$Cu_{15}Si_4$ geometry showing the mean dimensions, and (i) SEM image and corresponding EDX elemental mapping of Cu (red) and Si (green) distribution in the ρ-$Cu_{15}Si_4$.

The ρ-$Cu_{15}Si_4$ crystal structure was further examined in more detail by transmission electron microscopy (TEM) and X-ray diffraction (XRD) analysis. As shown in **Figure 2a-c**, the low resolution TEM images reveal the node-internode features and nonhollow structure of the stems, conforming with the FIB-SEM observations. However, the layered feature of the cup section is not clearly visible due to the high thickness resulting from overlap of the layers. High resolution TEM images (**Figure 2d** and **e**) of the cup section reveal the crystalline structure with a high degree of atomic ordering and an interplanar spacing of ~2.37 and ~2.22 Å for the (400) and (420) lattice orientations, respectively, as represented in **Figure 2f**. Similar crystalline features are also clearly observed in the stem section (**Figure S5)**, indicating that the crystal structure of ρ-$Cu_{15}Si_4$ is invariant across the cup and stem features. Selected area electron diffraction (SAED) patterns (inset) also show

discrete diffraction spots that match well with that of single crystal $Cu_{15}Si_4$ with a high degree of crystallinity.[14]

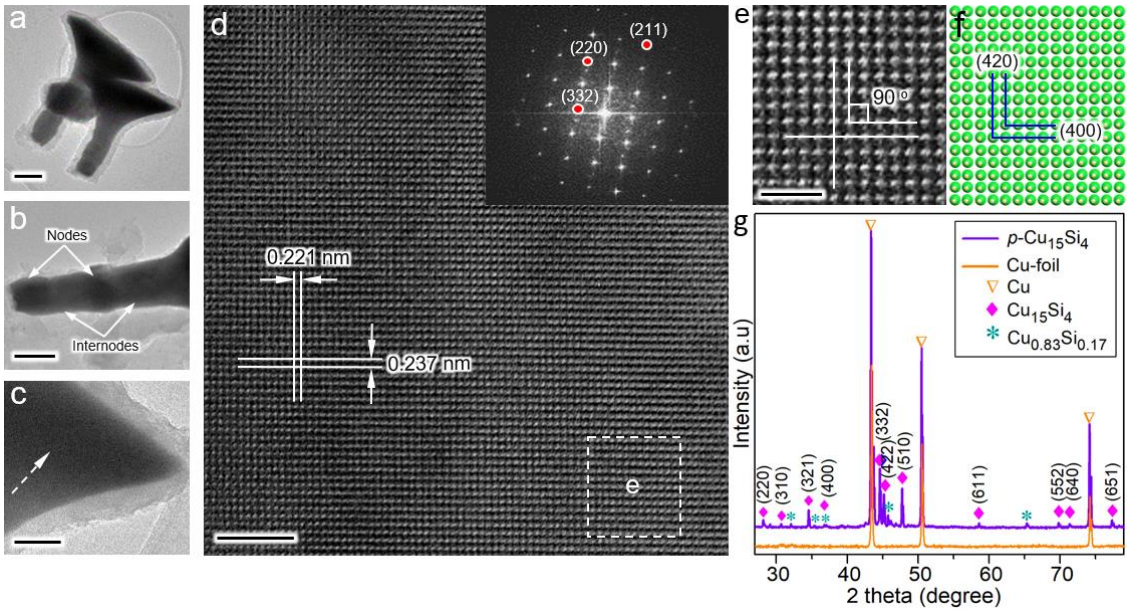

Figure 2 (a) Low resolution TEM image of the ρ-$Cu_{15}Si_4$ (scale: 200 nm) and magnified areas along the (b) stem and (c) cup sections (scale: 100 nm), (d) HR-TEM of the cup section (scale: 2 nm) and SAED pattern (inset), (e) Magnified image of the selected area marked by the dashed line in d (scale: 1 nm), and (f) representative model of atomic ordering, (g) X-ray diffraction patterns of ρ-$Cu_{15}Si_4$ and the parent Cu-foil.

X-ray diffraction patterns were also collected to verify the crystallinity of the ρ-$Cu_{15}Si_4$ structure. As shown in **Figure 2g**, the XRD pattern of ρ-$Cu_{15}Si_4$ matches with the diffraction characteristics of a typical $Cu_{15}Si_4$ phase (JCPDS: 01-076-1800) with a cubic crystal structure and $I\bar{4}3d$ space group.[14,23,26,35] Minor diffraction peaks assigned to $Cu_{0.83}Si_{0.17}$ (JCPDS: 00-023-0223) and intense peaks indexed to the parent Cu-foil (JCPDS: 01-070-3038) are also detected. However, the absence of the $Cu_{0.83}Si_{0.17}$ phase from the TEM analysis suggests that it only exists in a preformed silicide layer on the Cu-foil surface prior to the ρ-$Cu_{15}Si_4$ growth, conforming with the theory of intermediate state formation via a first-order phase transition.[32]

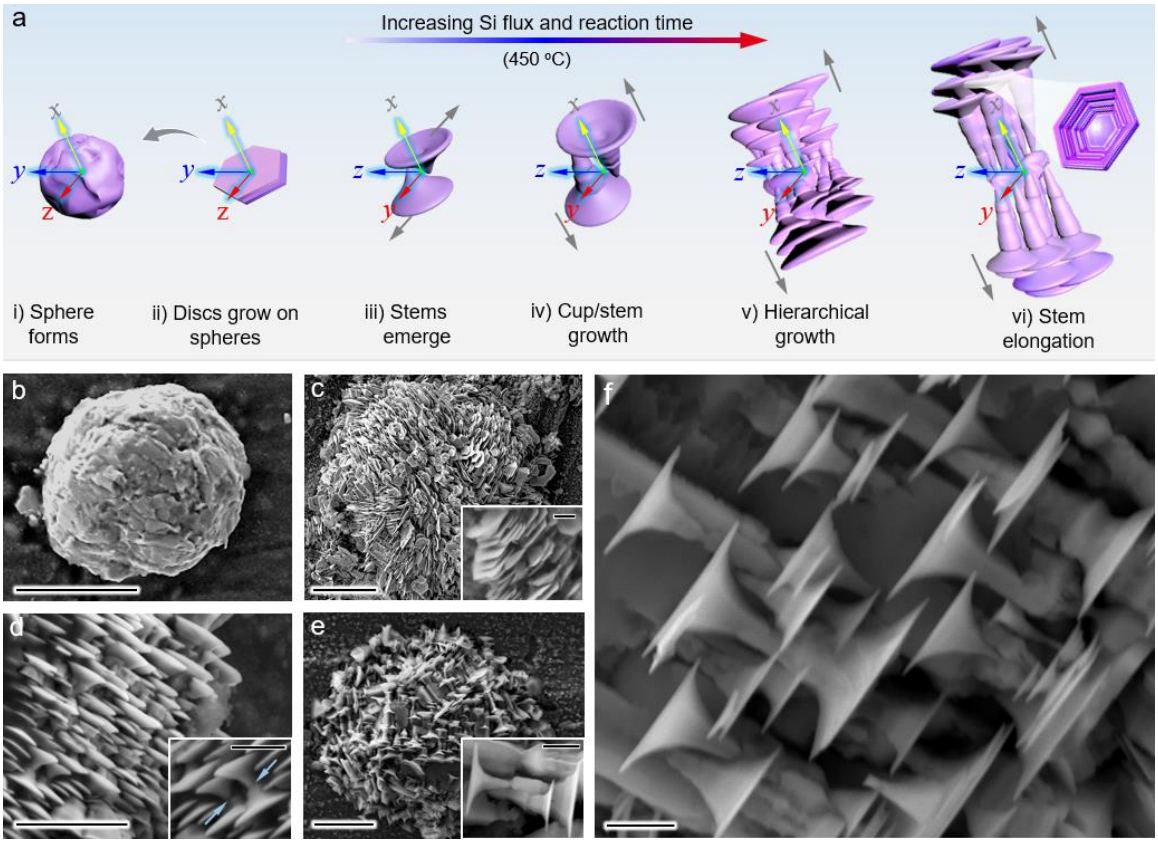

Figure 3 (a) Schematic illustration of the evolution sequence of the ρ-$Cu_{15}Si_4$: (*i*) spherical grains form first, (*ii*) pair of discs then form on the spherical grains surface, (*iii*) stems begin to emerge from the inner opposite faces of the discs, (*iv*) growth of stems and formation of the cup occur, (*v*) hierarchical growth, and (*vi*) finally the stems elongate in opposite directions. Gray arrows indicate growth directions along the *x*-axis, parallel to the growth substrate. SEM images of (b) spherical grains (scale: 10 µm), (c) hexagonal discs clusters grown on the spheres (scale: 10 µm), (d) enlarged image showing the emergence of the stems necking out in opposition directions (scale: 3 µm), and (e, f) cup-stem growth (scale: 10 and 1 µm, respectively).

Growth Mechanism of the ρ-$Cu_{15}Si_4$. The growth mechanism was qualitatively probed through *ex situ* experimental observations. It was revealed that the ρ-$Cu_{15}Si_4$ morphology evolves sequentially through the formation of Cu-rich silicide spheres followed by the surface evolution of hexagonal discs, stem growth, and then parallel elongation, as illustrated in **Figure 3a**. Typically, interatomic diffusion of Cu and Si atoms triggers the *in situ* formation of binary phase Cu-rich silicide spherical grains (**Figure 3b**), about ~13.7 µm in average size within ~30 min of reaction, which then serve as active sites (silicide islands) to facilitate further crystal growth. Although the Si monomer

decomposition was expected to occur uniformly on the substrate surface, the formation of the spherical grains is spontaneous (nonregulated) as is characteristic of nucleation events. The process of nucleation is typically random, with a high potential of occurrence at impurity or defect sites and grain boundaries,[36,37] and that may be accountable for the sparse distribution of the spherical grains as shown in **Figure S6**. After ~40 min of reaction, the formation of several pairs of hexagonal disc clusters on the spherical grains is observed (**Figure 3c**), increasing the overall size (*i.e.*, spherical grain and discs) to ~31.6 μm.

As demonstrated in **Figure S7**, the disc growth possibly evolves through a fluid−solid phase transformation mechanism at the interface between the Si flux and the spherical grains as Cu interdiffuses with Si atoms.[27,38] Atomic saturation of the interdiffused Cu/Si atoms induces coalescence, thereby, triggering crystallisation and growth at the crystallite grain surface. The continued reaction with the flux of Si leads to the gradual emergence of stems, protruding from the inner opposite faces between disc pairs, as shown in **Figure 3d**. This is facilitated by the diffusion of Cu from the Cu-rich crystallite spheres to react with Si, as suggested by slight decrease of the overall grain size from ~31.6 to ~22.5 μm (**Figure S8**). This phenomenon drives a diffusion-induced lateral growth and proliferation of interconnected disc-stem features, growing at exactly opposite sides of the growth crystal base with each set seemingly a reflected image of the other (**Figure 3e** and **f)**. Notably, the stems exhibit a comparable length as the disc size and a cone-like geometry consistent with the internode features observed in Figure 1 and 2.

Toward High Density Growth of the ρ-$Cu_{15}Si_4$. An electrochemical process was employed to pregrow discrete Cu crystals on the substrate surface prior to the ρ-$Cu_{15}Si_4$ growth. As shown in **Figure 4a** (inset figure), this process leads to the generation of pyramid-like Cu crystals that completely cover the Cu foil surface. As presented in **Figure 4a**, **b** and **S9**, the conversion of the Cu

crystals to Cu-silicide facilitates the subsequent growth of high density ρ-$Cu_{15}Si_4$ with enhanced surface coverage.

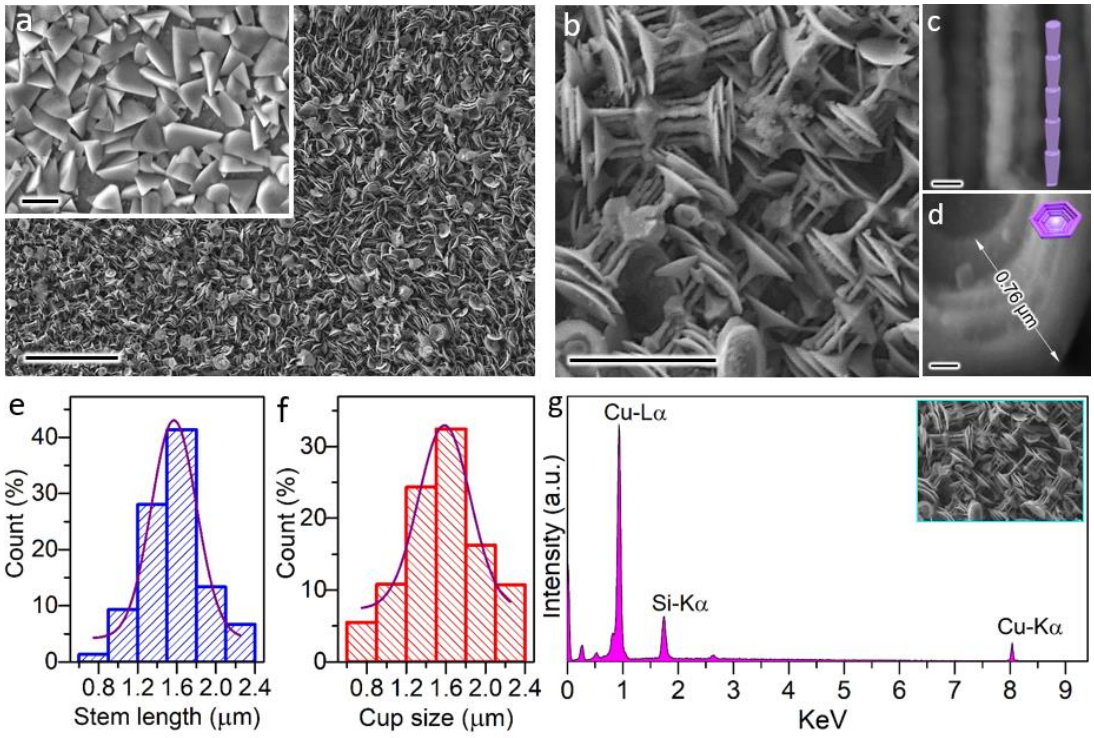

Figure 4 SEM images of (a, b) high density ρ-$Cu_{15}Si_4$ crystals in high yield at various magnifications (scale: 20 and 5 µm, respectively). An inset in figure *a* shows the electrochemically pre-grown Cu-crystals (scale: 2 µm), (c) node-internode feature of the stem (scale: 200 nm), (d) stairs-like layered feature of the cup section (scale: 200 nm), Gaussian-fitted size distribution histogram of the (e) cups (average size: ~1.47±0.7 µm) and (f) stems (average size: ~1.58 ± 0.8 µm), and (g) EDX spectrum of elemental composition (inset is the corresponding SEM image).

The average stem diameter remains at ~150 nm and extends by only ~2.25 µm in maximum length. However, the average cup size of ~1.47 µm is relatively higher, with a slight distortion of the hexagonal geometry. The occurrence of a relatively shorter stem length could be attributed to lateral growth hindrances, owing to limited growth space for continued elongation. This phenomenon leads to the fracture and slight displacement of the grown ρ-$Cu_{15}Si_4$ with excess reactants, resulting in the formation of small particles on the surfaces as seen in **Figure S10**. These observations may be due to

the high density and random orientations of the pregrown Cu-crystals that promote the high rate silicide growth. Regardless, the stems and cups also exhibit similar node-internode-like features (**Figure 4c**) and a layered morphology (**Figure 4d**) with a good size distribution as shown in panels **e** and **f of Figure 4** for the cups and stems, respectively. The EDX elemental spectrum (**Figure 4g**) also confirms the presence of both Cu and Si in the ρ-$Cu_{15}Si_4$ and the growth crystal base (**Figure S11**), indicating that the initial Cu-crystals have also been converted to Cu-silicide during the ρ-$Cu_{15}Si_4$ growth.

CONCLUSION

In summary, we show that a hierarchical ρ-$Cu_{15}Si_4$ nanoarchitecture can be laterally grown directly on a Cu-precursor substrate with morphologies consisting of small nanorods, stacked into 1D stems and terminated with concave hexagonally shaped 3D cups. While the stems exhibit node-internode-like features, the cups evolve through a self-regulated layer-by-layer deposition process. The growth mechanism suggests that the interdiffusion of Cu and Si atoms is the strongest driving force for the silicidation process, initially inducing the formation of Cu-rich silicide crystals as active growth islands. The growth orientation is independent of the underlying silicide crystal geometry (spherical or pyramidal) and is always lateral to the underlying substrate. Electrochemically pregrown Cu-crystals on the substrate also facilitate the direct growth of ρ-$Cu_{15}Si_4$ crystals in high yield with enhanced an substrate coverage. The results provide new routes and important insights into the growth mechanisms of nanoscale features in transition metal silicides that heretofore were not well understood and thus open new avenues to advance the development of TMS at a low cost for their wider application in electronic devices.

ASSOCIATED CONTENT

Supporting Information

Supporting Information. Details of the experimental section, characterisation methods and supplementary figures. This material is available free of charge via the Internet at:

AUTHOR INFORMATION

Corresponding author: E-mail: kevin.m.ryan@ul.ie, Phone: +353-61 213167

Author Contributions

All authors contributed to the manuscript and have approved of its content and submission.

Notes

The authors declare no competing financial interest.

Acknowledgments

I.S.A acknowledges funding from the European Union's Horizon 2020 research and innovation programme under the Marie Sklodowska-Curie Individual Fellowship Grant Agreement no: 843621. K.M.R acknowledges support by Science Foundation Ireland (SFI) under Grant Number 16/IA/4629 and the SFI Centers, MaREI, AMBER and Confirm, 12/RC/2302_P2, 12/RC/2278_P2 and 16/RC/3918, Irish Research Council (IRC) under Grant Number IRCLA/2017/285. H.G. acknowledges SIRG funding under Grant no. 18/SIRG/5484. M.D.S. and A.H. acknowledge support by the European Research Council (ERC) through a Starting Grant (Agreement no. 716792).

REFERENCES

(1) Schmitt, A. L.; Jin, S. Selective Patterned Growth of Silicide Nanowires without the Use of Metal Catalysts. *Chem. Mater*. **2007**, 19, 126-128.

(2) Schmitt, A. L.; Higgins, J. M.; Szczech, J. R.; Jin, S. Synthesis and Applications of Metal Silicide Nanowires *J. Mater. Chem*. **2010**, *20*, 223-235.

(3) Tsai, C.-I.; Yeh, P.-H.; Wang, C.-Y.; Wu, H.-W.; Chen, U.-S.; Lu, M.-Y.; Wu, W.-W.; Chen, L.-J.; Wang. Z.-L. Cobalt Silicide Nanostructures: Synthesis, Electron Transport, and Field Emission Properties. *Cryst. Growth Des*. **2009**, *9*, 4514 –4518.

(4) Chen, X.; Liang, C. Transition Metal Silicides: Fundamentals, Preparation and Catalytic Applications, *Catal. Sci. Technol*. **2019**, *9*, 4785-4820.

(5) Chen, L. J.; Wu, W. W.; Hsu, H. C.; Chen, S. Y.; Chueh, Y. L.; Chou, L. J.; Lu, K. C.; Tu, K. N. Metal Silicide Nanowires. *ECS Trans*. **2007**, *11*, 3−6.

(6) Seibt, M.; Griess, M.; Istratov, A. A.; Hedemann, H.; Sattler, A.; Schroter, W. Formation and Properties of Copper Silicide Precipitates in Silicon. *Phys. Status Solidi A* **1998**, *166*, 171−182.

(7) Chen, L. J.; Metal Silicides: An Integral Part of Microelectronics, *JOM* **2004**, *57*, 24-30.

(8) Buonassisi, T.; Marcus, M. A.; Istratov, A. A.; Heuer, M.; Ciszek, T. F.; Lai, B.; Cai, Z.; Weber, E. R. Analysis of Copper-Rich Precipitates in Silicon: Chemical State, Gettering, and Impact on Multicrystalline Silicon Solar Cell Material. *J. Appl. Phys*. **2005**, *97*, 063503-9.

(9) Li, C.-P.; Wang, N.; Wong, S.-P.; Lee, C.-S.; Lee, S.-T.; Metal Silicide/Silicon Nanowires from Metal Vapor Vacuum Arc Implantation. *Adv, Mater*. **2002**, *14*, 218–221.

(10) Wu, Y.; Xiang, J.; Yang, C.; Lu, W.; Lieber, C. M. Single-Crystal Metallic Nanowires and Metal/Semiconductor Nanowire Heterostructures. *Nature* **2004**, *430*, 61-65.

(11) Lin, Y.-C.; Chen, Y.; Huang, Y. The Growth and Applications of Silicides for Nanoscale Devices, *Nanoscale* **2012**, *4*, 1412-1421.

(12) Chueh, Y.-L.; Ko, M.-T.; Chou, L.-J.; Chen, L.-J.; Wu, C.-S.; Chen, C.-D. $TaSi_2$ Nanowires: A Potential Field Emitter and Interconnect. *Nano Lett*. **2006**, *6*, 1637–1644.

(13) Szczech, J. R.; Schmitt, A. L.; Bierman, M. J.; Jin, S. Single-Crystal Semiconducting Chromium Disilicide Nanowires Synthesized via Chemical Vapor Transport. *Chem. Mater*. **2007**, *19*, 13, 3238–3243.

(14) Geaney, H.; Dickinson, C.; O' Dwyer, C.; Mullane, E.; Singh, A.; Ryan, K. M. Growth of Crystalline Copper Silicide Nanowires in High Yield within a High Boiling Point Solvent System. *Chem. Mater*. **2012**, *24*, 4319 −4325.

(15) Sheehan, M.; Ramasse, Q. M.; Geaney, H.; Ryan. K. M. Linear Heterostructured Ni_2Si/Si Nanowires with Abrupt Interfaces Synthesised in Solution. *Nanoscale* **2018**, *10*, 19182-19187.

(16) Hou, Q. R.; Gu, B. F.; Chen, Y. B.; He, Y. J.; Sun, J. L. Layer-by-layer Deposition of $MnSi_{1.7}$ Film with high Seebeck Coefficient and Low Electrical Resistivity. *Mater. Chem*. *Phys*. **2014**, *146*, 346-353.

(17) Zhou, F.; Szczech, J.; Pettes, M. T.; Moore, A. L.; Jin, S.; Shi, L. Determination of Transport Properties in Chromium Disilicide Nanowires via Combined Thermoelectric and Structural Characterizations. *Nano Lett*. **2007**, *7*, 1649 –1654.

(18) Giannini, C.; Lagomarsino, S.; Scarinci, F.; Castrucci, P. Nature of the Band Gap of Polycrystalline *p*-$FeSi_2$ Films. *Phys. Rev. B*, **1992**, *45*, 8822–8824.

(19) Ahmed, S. J.; Boyer, C.; Niewczas, M. Magnetic and Structural Properties of Co_2MnSi based Heusler Compound. *J. Alloys Comp*. **2019**, *781*, 216–225.

(20) Hsu, H.-F.; Chen, C.-A.; Liu, S.-W.; Tang, C.-K. Fabrication and Gas-Sensing Properties of Ni-Silicide/Si Nanowires. *Nanoscale Res. Lett.* **2017**, *12*, 1–8.

(21) Lin, Y.-C., Lu, K.-C.; Wu, W.-W.; Bai, J.; Chen, L. J.; Tu, K. N.; Huang, Y. Single Crystalline PtSi Nanowires, PtSi/Si/PtSi Nanowire Heterostructures and Nanodevices. *Nano Lett*., **2008**, *8*, 913–918.

(22) Johnson, D. C.; Mosby, J. M.; Riha, S. C. Prieto, A. L. Synthesis of Copper Silicide Nanocrystallites Embedded in Silicon Nanowires for Enhanced Transport Properties. *J. Mater. Chem.* **2010**, *20*, 1993–1998.

(23) Stokes, K.; Geaney, H.; Sheehan, M.; Borsa, D.; Ryan, K. M. Copper Silicide Nanowires as Hosts for Amorphous Si Deposition as a Route to Produce High Capacity Lithium-Ion Battery Anodes. *Nano Lett*. **2019**, *19*, 8829−8835.

(24) Hymes, S.; Kumar, K. S.; Murarka, S. P.; Ding, P. J.; Wang, W.; Lanford, W. A. J.; Thermal Stability of Copper Silicide Passivation Layers in Copper-Based Multilevel Interconnects. *Appl. Phys*. **1998**, *83*, 4507–4512.

(25) Aminu, I. S.; Geaney, H.; Imtiaz , S.; Adegoke, T. E.; Kapuria, N.; Collins, G. A.; Ryan, K. M. A Copper Silicide Nanofoam Current Collector for Directly Grown Si Nanowire Networks and their Application as Lithium-Ion Anodes. *Adv. Funct. Mater*. **2020**, 2003278.

(26) Sufryd, K.; Ponweiser, N.; Riani, P.; Richter, K. W.; Cacciamani, G. Experimental Investigation of the Cu-Si Phase Diagram at *x*(Cu)>0.72. *Intermetallics* **2011**, *19*, 1479–1488.

(27) Jung, S.J; Lutz, T.; Bell, A. P.; McCarthy, E. K.; Boland, J. J. Free-Standing, Single-Crystal Cu_3Si Nanowires. *Cryst. Growth Des*. **2012**, *12*, 3076 −3081.

(28) Jung, S.J; O' Kelly, C. J.; Boland. J. J. Position Controlled Growth of Single Crystal Cu_3Si Nanostructures. *Cryst. Growth Des*. **2015**, *15*, 5355−5359.

(29) Li, S.; Cai, H.; Gan, C. L.; Guo, J.; Dong, Z.; Ma, J. Controlled Synthesis of Copper-Silicide Nanostructures. *Cryst. Growth Des*. **2010**, *10*, 2983– 2989.

(30) Zhang, Z.; Wong, L.M.; Ong, H.G.; Wang, X.J.; Wang, J. L.; Wang, S. J.; Chen, H.; Wu, T. Self-Assembled Shape- and Orientation-Controlled Synthesis of Nanoscale Cu_3Si Triangles, Squares, and Wires. *Nano Lett*. **2008**, *8*, 3205–3210.

(31) Kukushkin, S. A.; Osipov, A. V. First-Order Phase Transition through an Intermediate State. *Phys. Solid State*, **2014**, *56*, 792–800.

(32) Kukushkin, S. A.; Sakalo, T. V. Diffusional Coalescence of Island Films on the Real Crystal Surface in the Case of Layer-by-Layer Growth of Islands–I. An Isolated System. *Acta Metal. Mater*., **1993**, *41*, 1237–1241.

(33) Kukushkin, S. A.; Sakalo, T. V. Diffusional Coalescence of Island Films on the Real Crystal Surface in ihe Case of Layer-by-Layer Growth of Islands–II. An Open System. Undamped Sources of Deposited Atoms. *Acta Metal. Mater*., **1993**, *41*, 1243–1244.

(34) Sakalo, T. V.; Kukushkin, S. A. Diffusional Coalescence of Island Films on the Real Crystal Surface in ihe Case of Layer-by-Layer Growth of Islands–IV. Theory and Experiment. *Acta Metal. Mater*., **1994**, *42*, 2803–2810.

(35) Chromik, R. R.; Neils, W. K.; Cotts, E. J. Thermodynamic and kinetic study of Solid State Reactions in the Cu–Si System. *J. Appl. Phys*. **1999**, *86*, 4273–4281.

(36) Yizhi, Z.; Senbo, X.; Verner, H.; Jianying, H.; Zhiliang, Z.; Anti-icing Ionogel Surfaces: Inhibiting Ice Nucleation, Growth, and Adhesion, *ACS Materials Lett*. **2020**, *2*, 616−623.

(37) P. D. Kanungo, R. Koegler, N. Zakharov, P. Werner, R. Scholz, W. Skorupa, Characterization of Structural Changes Associated with Doping Silicon Nanowires by Ion Implantation. *Cryst. Growth Des*. 2011, **11**, 2690 –2694.

(38) Li, J.; Wang, Z.; Deepak, F. L. In Situ Atomic-Scale Observation of Droplet Coalescence Driven Nucleation and Growth at Liquid/Solid Interfaces. *ACS Nano* **2017**, *11*, 5590 −5597.

For Table of Contents Use Only

Evolution of Hierarchically-Layered Cu-rich Silicide Nano-Architectures

Ibrahim Saana Amiinu, Nilotpal Kapuria, Temilade Esther Adegoke, Angelika Holzinger, Hugh Geaney, Micheál D. Scanlon, Kevin M. Ryan*

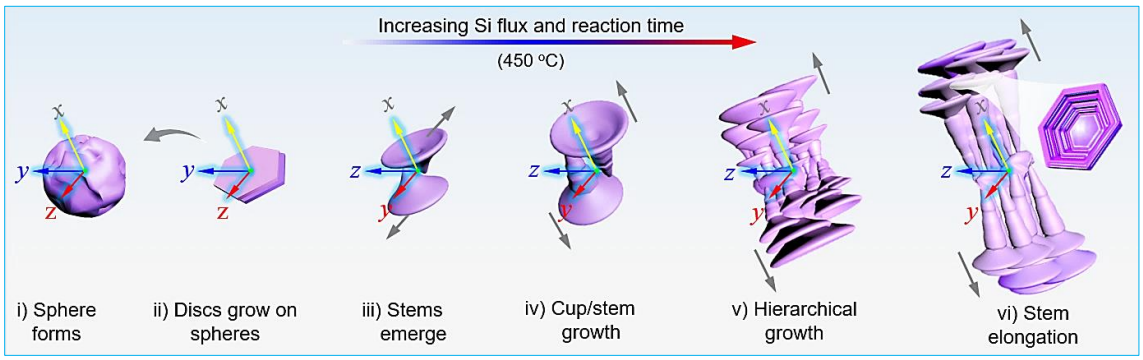

Synopsis

A Cu rich silicide nanoarchitecture (ρ-$Cu_{15}Si_4$), consisting of a stack of nanorods (~300 nm in length) and terminated with concave hexagonal 3D cups that evolve through a self-regulated layer-by-layer growth mechanism is demonstrated. The structural evolution is governed by interatomic diffusion, initially triggering the formation of binary-phase silicide islands (spheres) followed by the formation of hexagonal discs, stem growth, and lateral elongation in exactly opposite directions.